APPLIED SCIENCES AND ENGINEERING

Three-dimensional printing of wood

Md Shajedul Hoque Thakur[1]†, Chen Shi[1]†, Logan T. Kearney[2], M. A. S. R. Saadi[1], Matthew D. Meyer[3], Amit K. Naskar[2], Pulickel M. Ajayan[1], Muhammad M. Rahman[1]*

Copyright © 2024 The Authors, some rights reserved; exclusive licensee American Association for the Advancement of Science. No claim to original U.S. Government Works. Distributed under a Creative Commons Attribution NonCommercial License 4.0 (CC BY-NC).

Natural wood has served as a foundational material for buildings, furniture, and architectural structures for millennia, typically shaped through subtractive manufacturing techniques. However, this process often generates substantial wood waste, leading to material inefficiency and increased production costs. A potential opportunity arises if complex wood structures can be created through additive processes. Here, we demonstrate an additive-free, water-based ink made of lignin and cellulose, the primary building blocks of natural wood, that can be used to three-dimensional (3D) print architecturally designed wood structures via direct ink writing. The resulting printed structures, after heat treatment, closely resemble the visual, textural, olfactory, and macro-anisotropic properties, including mechanical properties, of natural wood. Our results pave the way for 3D-printed wooden construction with a sustainable pathway to upcycle/recycle natural wood.

INTRODUCTION

For countless centuries, natural wood has served as a fundamental material for a wide variety of purposes, encompassing the construction of buildings, the manufacturing of furniture, and the creation of architectural structures (*1*, *2*). Traditionally, wood shaping has relied on subtractive manufacturing techniques. However, this process often generates a substantial amount of waste material, resulting in material wastage and increased production costs. In light of the growing concerns surrounding sustainability and the need for effective waste management, recycling waste wood has become imperative (*3*–*5*). Currently, the recycling of waste wood is primarily constrained to its traditional uses, such as fuel, mulch, filler for particleboards, sewage sludge fill medium, compost, and animal bedding. However, it is important to recognize that waste wood has untapped potential as it can be deconstructed into its fundamental building blocks. The smallest microstructural component of wood is called a microfibril, which is a bundle of cellulose chains having both crystalline and amorphous regions covered by lignin. Its composition includes cellulosic carbohydrates (~70%) as reinforcements and lignin (~25%) as a continuous phase, along with other minor components (*6*). Typically, they serve as valuable resources to produce various bio-based materials for functional and structural applications (*7*–*19*). Lignin is one of the most abundant biopolymers on Earth. Found primarily in plant cell walls, it is also the least-valued product in industries such as commercial paper mills and biorefineries (*20*–*22*). Cellulose, on the other hand, is a versatile polysaccharide with great potential, especially because it can be transformed into nanocellulose, a nanomaterial with exceptional mechanical properties, which opens up possibilities for applications in high-performance bio-based structures (*16*, *23*, *24*). We are exploring the prospect of recombining these bio-based materials (lignin and cellulose nanomaterials), abundantly available in waste wood, to fabricate wood structures in a bottom-up approach rather than the traditional top-down method discussed above.

Additive manufacturing (AM), also known as three-dimensional (3D) printing, is the latest manufacturing technology that builds objects layer by layer in a bottom-up approach. The technique reduces considerable material waste as it only uses the necessary amount of material for the object being created. It also facilitates unprecedented design freedom with its ability to create highly intricate architected structures (*25*, *26*). Some attempts have been made to use waste wood in the AM by combining wood powder/sawdust with binders, typically synthetic or bio-resins, to make 3D printable feedstocks (*27*–*29*). Nevertheless, the end products of these fused filament fabrication–based works are typically polymer composites without mimicking the actual wood composition. The stereolithography technique has also been adopted for the 3D printing of wood (*30*). However, a toxic solvent such as acetone was used in the process. Another AM technique, direct ink writing (DIW), has emerged as one of the most versatile methods to enable the 3D printing of a wide variety of materials (*24*, *31*). DIW is an extrusion-based AM technique that allows the 3D printing of any material composition as long as the precursor ink can be engineered to demonstrate appropriate rheological behavior. Consequently, in recent years, researchers have attempted to 3D print structures via DIW by using some of the individual building blocks of wood (*32*–*35*). For example, Jiang *et al.* (*34*) used DIW to print lignin-based structures mixed with Pluronic F127. Zhang *et al.* (*36*) printed cellulose nanofibers (CNFs) and alginate with a very small amount of colloidal lignin particles [0.5 weight % (wt %)] using DIW for soft tissue engineering. Some attempts have also been made to 3D print lignin by combining it with hydroxypropyl cellulose. However, either only ring-like structures could be printed (*37*) or the printed structures had insufficient shape fidelity (deviation from intended dimensions) (*38*). Researchers have also investigated the possibility of printing lignin combined with cellulose fibers (*39*) or binders such as methylcellulose (*40*). Yet, the printed structures showed uneven shrinkage during drying, leading to large shape changes, and the printing resolution was also low, thus leading to thick layers and large interlayer separations. However, combining lignin with CNF and nanocrystal reinforcement phases to replicate natural wood composition while ensuring high-resolution printability and fabricating architected structures is challenging and has not been reported in the literature.

[1]Department of Materials Science and NanoEngineering, Rice University, Houston, TX, USA. [2]Chemical Sciences Division, Oak Ridge National Laboratory, Oak Ridge, TN, USA. [3]Shared Equipment Authority, Rice University, Houston, TX, USA.
*Corresponding author. Email: maksud@rice.edu
†These authors contributed equally to this work.

Downloaded from https://www.science.org on April 03, 2024

Here, we formulate a water-based viscoelastic ink using these two primary wood building blocks: lignin and cellulose, to facilitate the 3D printing of complex wood structures at room temperature using DIW. We use both cellulose nanocrystals (CNCs) and CNF to replicate the crystalline and amorphous part of cellulose present in natural wood. The ink has entirely wood-based constituents and is devoid of any binder or foreign polymeric phase. We find the optimal composition of the constituents to be very similar to that of natural wood, which also provides the appropriate rheology to enable the printing of highly intricate architected structures—a key characteristic of AM. The 3D-printed wood has the appearance, mechanical properties, thermal stability, and olfactory characteristics similar to those of natural balsa wood. The utilization of nanoscale building blocks through DIW for 3D printing wood offers a potential and sustainable pathway for wood recycling, intricate wood architecture, and the integration of mechanical reinforcements within wooden structures.

RESULTS

The ink comprises CNCs, tempo-oxidized CNFs (TOCNs), and hardwood lignin. TEM images, measuring the dimensions of the cellulose nanomaterials used in this study, are presented in fig. S1. The CNCs were mostly arranged into filamentous structures that were generally 100 to 700 nm in length. The TOCN fibers were about 200 to 480 nm in length and 7 to 9 nm wide. Scanning electron microscopy (SEM) images (fig. S2) reveal the dimensions of the lignin powder used in the ink. The lignin particles had irregular shapes with diameters varying between 1 to 12 μm. TOCN, CNC, and lignin interact with each other based on their morphology, hydrogen bonding intensity, and solution-regulated self-assembly. However, there is no notable change in the crystal structure of the constituents during mixing formulation (see the Supplementary Materials). TOCN, with its high aspect ratio and chemically modified hydrogen bonding moieties, forms an interconnected meso-structure through physical entanglements. The interconnected meso-structure acts as a dilated scaffold to hold the accompanying components within. CNCs, on the other hand, with their exceptional rigidity and lyotropic liquid crystallinity, form stiff reinforcing phases to underpin the mechanical properties. The CNCs used were in an aqueous solution, and the water from the solution acts as a molecular plasticizer to induce the rheology required for DIW while also ensuring a homogenous distribution of the components within the ink. Last, when the printed part is heated, the lignin, due to its innate thermoplastic response, behaves as a molecular glue to fill voids, thereby bridging the cellulose-based components into a cohesive self-assembled structure. Thus, these components that make up natural wood are turned into sustainable 3D-printed wooden architectures by extruding the ink through a DIW printer (fig. S4), followed by some hot processing that will be discussed later. A schematic conceptualization of the 3D printing of wood structures from the basic building blocks of natural wood is presented in Fig. 1A. The proposed procedure is also recyclable, as demonstrated in fig. S5. Using the presented scheme, 3D printing of wood structures at a high resolution, including miniature furniture and complex architectures (rectilinear, honeycomb, and Rice logo) has been achieved (Fig. 1B). Parts can also be separately printed and assembled into desired structures, such as the four-legged table shown in Fig. 1B.

A crucial element in creating a wood-based viscoelastic ink is to ensure that its rheology allows it to be consistently extruded through a high gauge nozzle at ambient conditions without requiring high pressure in the syringe (*24*). We were able to formulate an additive-free viscoelastic ink, representing wood composition, with rheological properties conducive to DIW (see Materials and Methods). The goal was to extrude the additive-free, stable aqueous ink through a 25-gauge nozzle under reasonable syringe pressure at ambient conditions (fig. S4). The usage of a 25-gauge nozzle ensures that the printing resolution could be as high as 200 μm. Figure 2A presents optical micrographs of the layer-by-layer structures, demonstrating the resolution from the top and front view, respectively. The interlayer separation is less than 100 μm. While optimizing the ink formulation, the lignin composition was kept constant at 25 wt % to mimic natural wood constituents (*6*). The ratio of the remaining constituents, CNC and TOCN, was extensively varied to determine the printable regime, as shown in Fig. 2B. The optimized ink had 37.5 wt % of both CNC and TOCN, which demonstrated shear-thinning behavior, as seen from the viscosity versus shear rate results (Fig. 2C). The ink shows a power law index, n, of 0.138, which is close to that of clay ($n = 0.12$), a material with one of the most appropriate rheology for DIW (*24*). The ink also undergoes a transition from viscoelastic solid to viscoelastic liquid under high shear strain, as shown in Fig. 2D. At high oscillatory strain, the loss modulus is higher than the storage modulus, demonstrating the ink's ability to flow within the nozzle. Meanwhile, at low oscillatory strain, the storage modulus is greater than the loss modulus, indicating the ability of the ink to retain its shape outside the nozzle after extrusion. These characteristics ensure that the rheology of the ink is conducive to DIW, enabling the 3D printing of complex wood structures.

Generally, the thermal stability of wood is of utmost importance as it ensures the material's resistance to warping, cracking, and structural degradation, making it a durable and reliable choice for a wide range of applications, from construction to furniture crafting. We performed a thermogravimetric analysis (TGA) to investigate the 3D-printed wood's thermal response and stability compared to natural wood. Three important parameters are investigated from the TGA results, namely, remaining mass fraction (wt %), degree of decomposition (α), and the mass fraction loss rate, also known as derivative TGA (DTGA). The methods used to calculate these parameters are given in the Supplementary Materials. We carried out TGA on the individual components of the ink, the 3D-printed wood, and natural wood, as shown in figs. S6 and 2E, respectively. The results from the individual components agree with that of the printed wood, indicating no major change in the material's thermal stability during postprocessing. When comparing the TGA of natural wood to that of our 3D-printed wood, we observe similar thermal stability, with both materials undergoing thermal degradation around 250°C, as shown in Fig. 2E. The mass fraction loss rates also peak around the same temperatures for printed wood composition and natural wood, as presented in Fig. 2F. However, the printed wood shows a lower peak, indicating a slower thermal degradation as compared to the natural wood. The initial degradation, peak derivative temperature, and char yield of printed and natural wood, as measured from the thermal degradation curves, are compared in table S1. The onset of degradation corresponds to the inflection point of the curve, decomposition temperature is defined as the point by which the majority of the weight loss has already occurred, and the residual mass is the char yield after heating to 800°C. The

Downloaded from https://www.science.org on April 03, 2024

Fig. 1. Process schematic showing 3D printing of wood architectures. (**A**) Schematic of the wood printing process. (**B**) Printed samples of various architectures. From the left: A one-legged table with a chair, top view of the table showing a honeycomb architecture with the Rice University R logo in the middle, the chair behind a four-legged table (legs printed and assembled separately), top views of a honeycomb, a rectilinear structure, and the letters WOOD.

printed composition does not use any C5 carbohydrate, which is common in any natural wood; thus, it undergoes slower degradation than natural wood while delivering 15.4% more charred residue at high temperatures.

Next, we investigated the microstructure of the 3D-printed wood. To achieve a 3D-printed wood structure resembling natural wood, a few steps need to be performed after printing. Figure 3 shows the schematic of the DIW printing and subsequent processing steps. As the water of the aqueous CNC solution remains in the printed structure in the form of moisture, it must be removed while also ensuring that the structure is not compromised because of any plasticization or flow. Drying in ambient conditions leads to uncontrolled deformation and bending that affects the dimensions of the print while also leading to cracks within the structure. To avoid such structural deformation, lyophilization has been adopted. The samples are freeze-dried at −80°C under vacuum (<1-mbar pressure) to remove the moisture (74% mass reduction) while retaining the size and shape of the printed part. After moisture removal, the samples were then subjected to a high-temperature treatment (at 180°C) that is proposed to lead to the melting and resolidification of the hardwood lignin, termed lignin fusion. The use of devolatilized lignin (*41*) helps retain the shape of the structure without creating gaseous products. Lignin undergoes softening way below 180°C as shown by the softening point characterization in fig. S7. Therefore, at 180°C, the lignin can flow inside the structure and bind the other components. Further evidence for this lignin fusion can be seen in the SEM images before and after heat treatment in Fig. 3 (A to C), as the gaps or voids between the layers are reduced by more than ~50% after the heat treatment. The heat treatment process reduces voids in the structure without altering the size and shape. Thus, we are able to ensure that the 3D-printed architected wood structures are nearly void-free solids after heat treatment.

To further densify and consolidate the 3D-printed wood structures to enhance their mechanical properties, the samples were

Downloaded from https://www.science.org on April 03, 2024

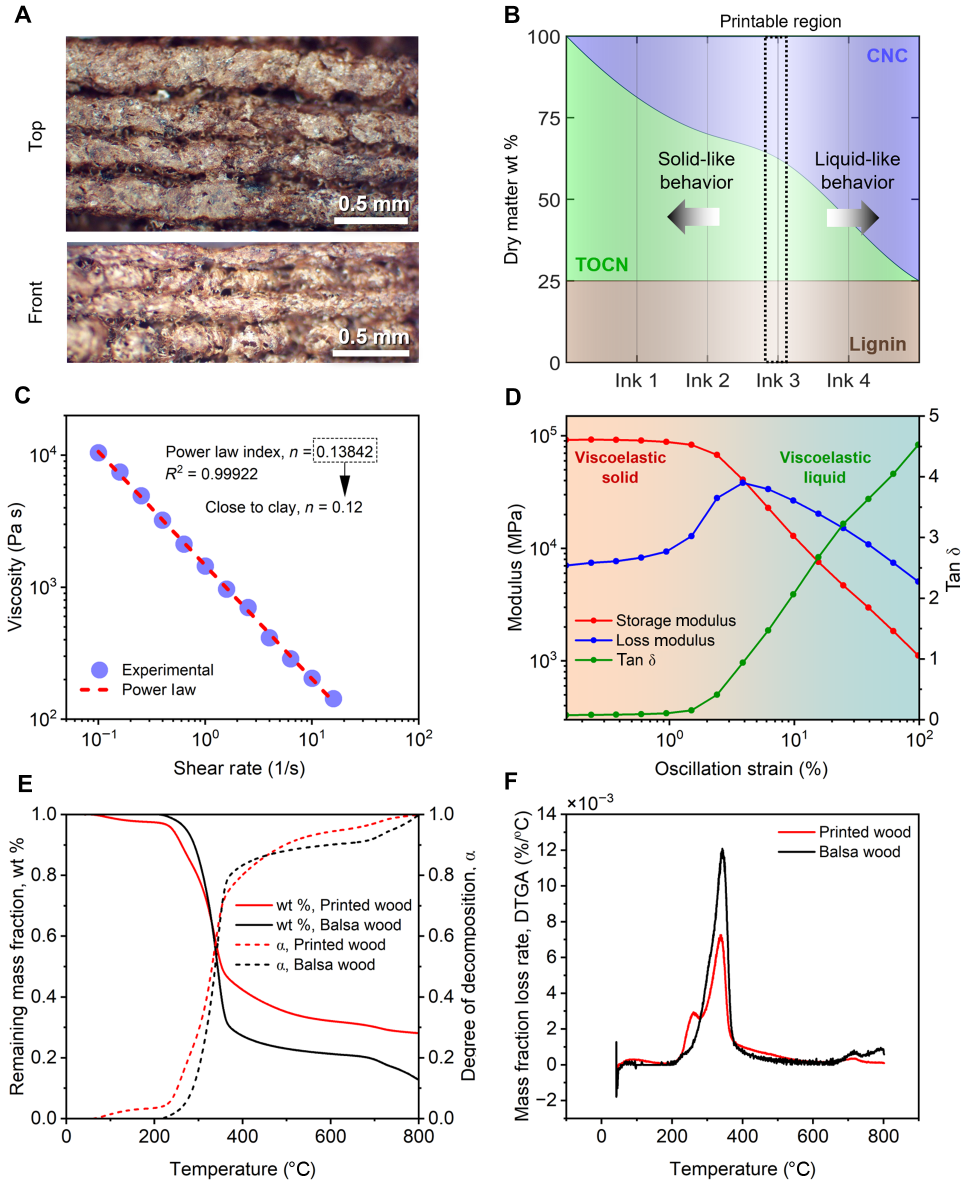

Fig. 2. Rheology study for direct ink writing (DIW) and thermal stability of printed wood. (**A**) Layer-by-layer assembly of the 3D-printed wood seen under an optical microscope, top view, and front view, respectively. (**B**) The printability of various ink compositions with respect to their dry matter weight percentages. (**C**) Ink viscosity as a function of shear rate, showing shear thinning behavior with a power law index, $n = 0.13842$. (**D**) Loss modulus, storage modulus, and tan δ as a function of oscillation strain amplitude. A transition from viscoelastic solid to viscoelastic liquid behavior is observed as the storage modulus decreases below the loss modulus, raising the tan δ above 1. (**E**) Thermogravimetric analysis (TGA) comparison of 3D-printed and natural balsa wood. Nearly equivalent thermal mass loss occurs within the 200° to 380°C range for both 3D-printed and natural wood, indicating similar thermal stability. (**F**) The mass fraction loss rate, also known as derivative TGA (DTGA), of the 3D-printed wood compared to the similar natural wood.

hot-pressed orthogonal to the printing direction. All samples as printed are aligned in the *x* direction and printed from the *x*-*y* plane to a higher *z* (Fig. 3D). We compared unpressed, single-pressed (two types), and double-pressed (two types) samples. Thus, five types of samples were prepared: unpressed, pressed in Y, pressed in Z, pressed in Z then Y (Z&Y), and pressed in Y then Z (Y&Z). For example, in table S2, all the samples are printed at dimensions such that, after pressing, they have the same dimensions of 9 mm × 9 mm × 9 mm. The hot-pressed samples have a further reduction in the gap between the layers, as can be seen in Fig. 3 (C and G). This also leads to a morphology very similar to that of the natural wood. SEM images of the microstructures of the natural wood and the hot-pressed sample are compared in Fig. 3 (E to G). Natural wood has a highly oriented structure resulting from its directionally biased growth (*42*, *43*), and the 3D-printed wood also shows a similar alignment of layers, as well as a similar gap between the layers, after undergoing the hot-press treatment. Although we are starting with the same nanoscale building blocks as that of natural wood,

Downloaded from https://www.science.org on April 03, 2024

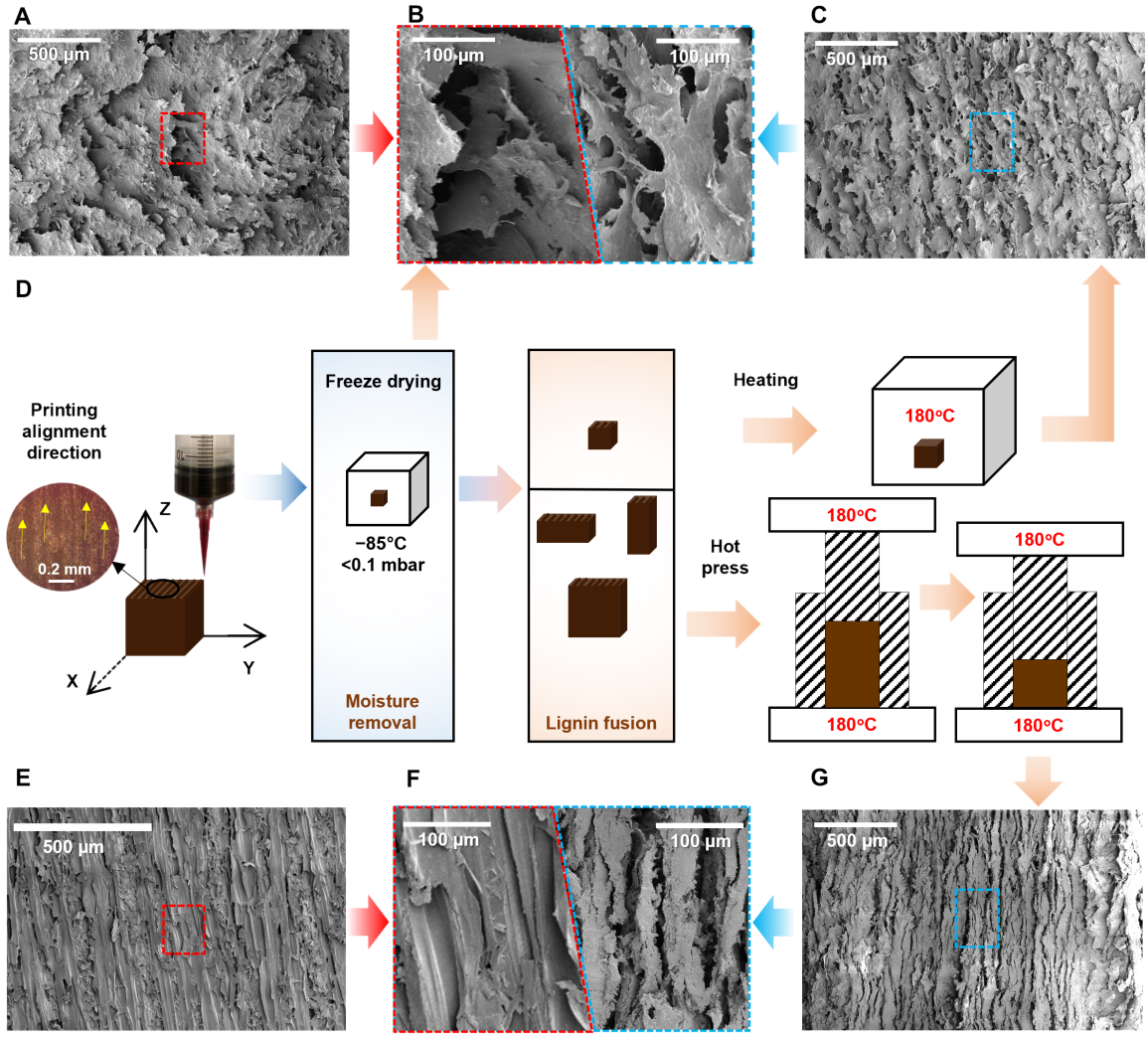

Fig. 3. Microstructures after printing and post-printing operations. (**A** to **C**) Cross-section SEM images on the *x-y* plane of the (A) unheated and (C) heated samples. Higher magnification SEM images of inset areas (dotted) of (A) and (C) are shown on the left and right sides of (B), respectively. The spacing between the layers is reduced because of lignin fusion during heating. (**D**) Schematic of the sample preparation steps. At first, structures are 3D-printed using an extrusion-based DIW technique. The shear force during extrusion provides alignment to the samples in the printing direction. Next, the samples are freeze-dried at −85°C and <0.1-mbar pressure to remove moisture that was introduced from the CNC. Last, the samples undergo either heating in the oven or hot press at 180°C to induce lignin fusion. (**E** to **G**) Cross-section SEM images on the *x-y* plane of the natural wood (E) and the final hot-pressed samples (G). Higher magnification SEM images of inset areas (dotted) of (E) and (G) are shown on the left and right sides of (F), respectively. A similar alignment between the layers and a similar gap between the layers is observed.

arbitrary mixing cannot produce directionally oriented structures due to the lack of a natural growth mechanism. Yet, we see macroscopic alignment in the 3D-printed wood due to the shear force in the nozzle during extrusion. Although the 3D printing and hot-pressing processes give the samples a macroscopic structural anisotropy, the internal structure remains isotropic in the nanoscale. The nanoscale isotropy ensures that the 3D printing process can predictably generate arbitrarily complex parts with isotropic shrinkage while maintaining the macroscale anisotropy induced by the printing direction, as observed above. To investigate this, we carried out wide-angle x-ray scattering (WAXS) on the printed wood, and no anisotropic peaks were observed. In fig. S3, the scattering pattern of the ink is compared to those of the printed parts at various stages of processing. Unlike well-studied natural woods, we observe no anisotropy in the scattering pattern, where the cellulosic domains are oriented along a primary growth direction. The residual water in the ink produces a strong broad scattering peak (*44*), which is eliminated following the freeze-drying step. However, following the freeze-drying step, no further structural changes are observed in the WAXS regime, regardless of pressing direction or the application of heat. The internal structure remains isotropic despite all processing.

For practical applications of wood, the most critical parameters are mechanical properties, such as compressive and flexural. Processing steps that induce directionality or densification can substantially affect the mechanical properties. In our case, the DIW method helps bring about macroscale anisotropy in the structure due to the shear force during extrusion. On the other hand, the subsequent hot-press method densifies the structure, induces lignin fusion, and

Downloaded from https://www.science.org on April 03, 2024

enhances the structure's directionality. To investigate the abovementioned processing-structure-property relationship of the 3D-printed wood, we carried out compression and three-point bending tests and compared the results with that of natural wood. The results from the compression tests are presented in Fig. 4A and fig. S8A. All tests were carried out along the printing direction for printed samples and the fiber alignment direction for the natural wood. The changes in mechanical properties due to a single hot press (pressed in Y or Z samples) were insignificant and within the error bar range. However, it is observed that the double-pressed samples (Y&Z and

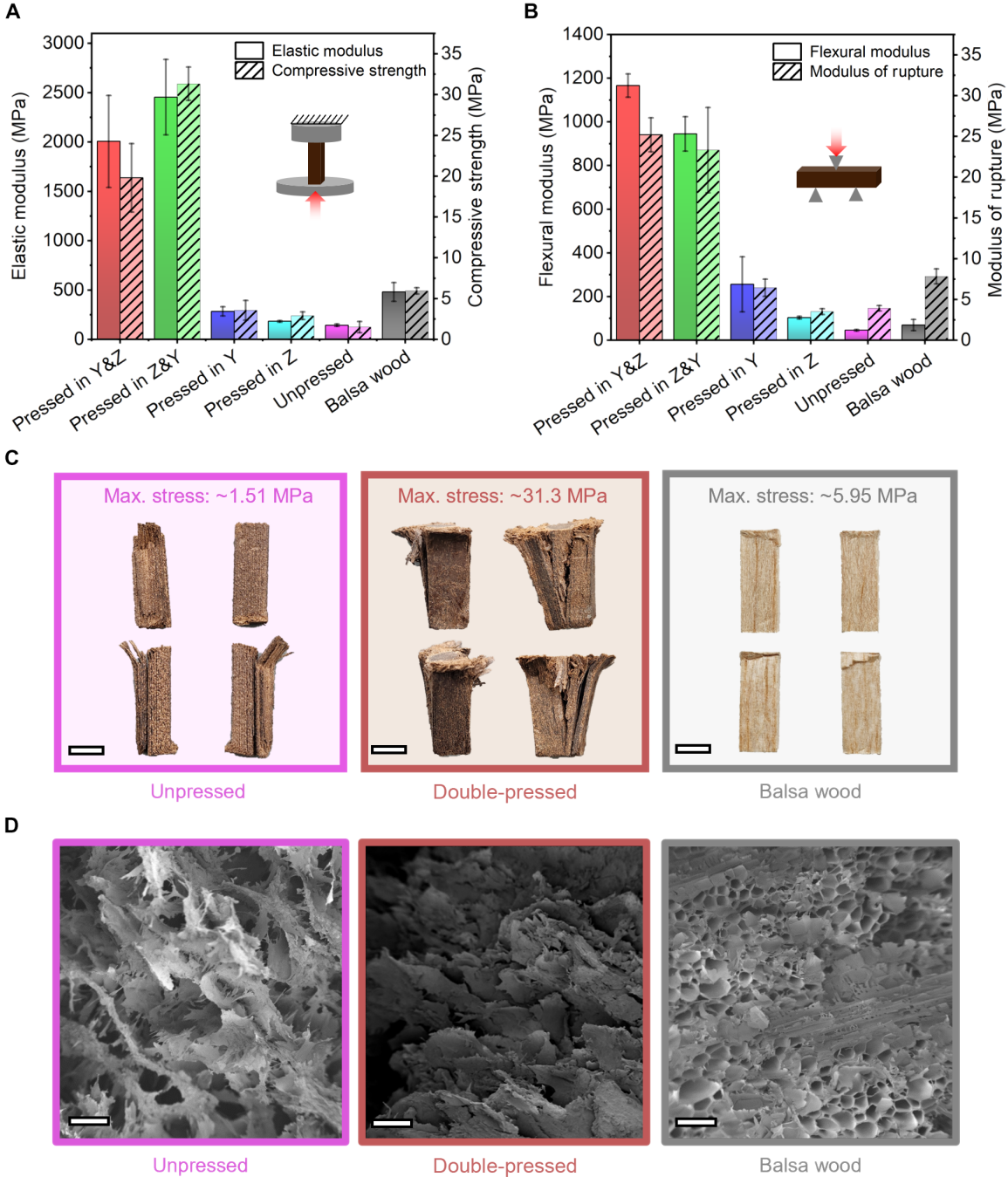

Fig. 4. Mechanical properties of 3D-printed wood. Bar plot showing the comparison of (**A**) compressive (elastic moduli and compressive strengths) and (**B**) flexure (modulus of rupture and flexural modulus) properties of the unpressed and hot-pressed 3D-printed wood and natural balsa wood. Inset: Schematic of (A) the compression test and (B) the flexure test setup configuration. (**C**) Optical photographs showing four views of fractured 3D-printed unpressed, double-pressed, and balsa wood after compression test. Scale bars, 5 mm. (**D**) SEM images (left to right) of the flexure fracture surfaces of unpressed and double-pressed 3D-printed wood and natural balsa wood, respectively. Scale bars, 100 μm.

Downloaded from https://www.science.org on April 03, 2024

Z&Y) had the highest ultimate compressive strength. The failure modes of the unpressed, double-pressed, and balsa samples were also different (Fig. 4C). The unpressed 3D-printed wood shows a split failure at ~1.51 MPa as the layers separate due to the layer-by-layer printing process. On the other hand, the balsa wood shows a shear failure mode at ~5.95 MPa with staircase-like cracks inclined at ~45°. The double-pressed 3D-printed wood, however, shows a wedge-split failure with a failure at a remarkably higher stress level (31.3 MPa) as it is much stiffer and stronger than balsa wood. Compared to natural balsa wood, the double-pressed Y&Z and Z&Y samples showed 182 and 162% enhancement in compressive strength, respectively (Fig. 4A). The increase in strength can be attributed to the densification during hot-press and the macroscopic alignment induced in the extrusion direction during DIW. Evidently, from fig. S8A, higher compression energy is absorbed by the double-pressed samples, which can be attributed to the lignin fusion consolidating most voids within the structure that was present before hot-pressing. This was also apparent from the SEM images in Fig. 3 (A to C and G), where the spacing between the printed layers and overall voids in the 3D structure was considerably reduced by the heat treatment and hot-press methods. This indicates that when using hot-pressing as a processing step for suitable designs, applying pressure in both directions (bidirectional pressing) is preferable over applying pressure in only one direction. However, hot-pressing might not be suitable for the postprocessing of certain 3D-printed architected structures. Thus, as of now, the abovementioned benefits of hot-pressing cannot be achieved in the architected samples. Regardless, these 3D-printed architected wood structures could be just as suitable as natural wood for specific applications such as decorative, recreational, and disposable utensils.

Another mechanical property necessary in structural applications is the flexural stress-strain response, which has been investigated via three-point bending tests, as presented in Fig. 4B. While the flexural stress-strain responses of the unpressed samples are not as good as the natural wood, both the Y&Z-pressed and the Z&Y-pressed 3D-printed samples readily surpass the natural wood in terms of both modulus of rupture and flexural modulus. Compared to natural balsa wood, the double-pressed Y&Z and Z&Y samples showed 222 and 198% enhancement in modulus of rupture and 1571 and 1254% enhancement in flexural modulus, respectively (Fig. 4B).

To better understand the mechanics behind these enhancements, the fracture surfaces of the samples were analyzed using high-resolution SEM. In Fig. 4D, from the fracture surfaces, we can see that the natural wood has a cellular architecture with quasi-regular pores. On the other hand, the cellular architecture of unpressed 3D-printed wood has a stochastic porosity, and the double-pressed 3D-printed wood has a dense/compact nearly homogeneous structure. The regularly arranged pores and voids in natural balsa wood act as energy absorption sites (*45*), thus leading to large flexure strains. On the contrary, the mechanical response of the unpressed 3D-printed sample is complicated because of its stochastic porosity (*46*), and in this case, it has led to lower strength and ductility. However, in the double-pressed 3D-printed wood, the increase in density leads to a stronger and less compliant structure. This is similar to the effect of densification on other cellular materials, including natural wood (*47*). When cellular materials undergo densification, the pores and voids are removed, thus leading to lower energy absorption but higher strengths. Another parameter that affects the flexure properties is the fully aligned long natural fibers, which act as mechanical reinforcements in balsa wood. In contrast, the fibers used in our ink formulation are in the range of a few hundred nanometers. Thus, introducing long natural fibers into the ink composition can be a possible technique to further enhance the mechanical properties of the 3D-printed wood, which can be explored in future endeavors. In addition, other organic and inorganic fillers may also be introduced into the ink formulation to generate mechanically robust and functional hybrid 3D-printed wood structures. The aesthetic attributes of the 3D-printed wood can also be enhanced by common postprocessing techniques, such as paints, laminates, and varnish, to mimic the grains of a wide variety of wood species. Another aspect that can be explored in the future is that the 3D printing wood ink constituents can also be sourced from other low-cost green resources. For instance, one can take cellulose produced by living organisms, such as bacteria (*48*), tunicates (*49*), and agro-waste (*50*), and lignin from any vascular plants/trees such as cotton, jute, and hemp (*51*), and can 3D print wood structures.

DISCUSSION

To summarize, we have developed an ink formulation that facilitated the 3D printing of wood using DIW from its nanoscale building blocks, enabling the fabrication of architected 3D wood structures. The ink components are entirely reusable and can all be extracted from waste wood, highlighting the recyclability and sustainability of the process. The thermal stability, constituents, texture, appearance, and olfactory characteristics of 3D-printed woods are all akin to those of natural wood. The mechanical properties are close to those of natural wood and can be further enhanced through the introduction of various fibers and other reinforcements into the ink formulation. Although the materials used in this work are all sourced from sustainable resources, we do use energy-intensive processes: freeze-dry and hot-press. Therefore, a more complete understanding of the sustainability of the process requires techno-economic analysis and life-cycle assessments in the future. Also, while scaling up the process, further experimental investigations are required on extrusion parameters, ink formulations and rheology, and overhang limits for complex architecture-scale structures. Nonetheless, this technique of 3D printing wood using nanoscale building blocks via DIW can pave the pathway for the recycling of wood, realizing complex architected wood structures, and developing mechanically robust and functional hybrid 3D-printed wood structures.

MATERIALS AND METHODS

Materials

Natural wood used in this work is balsa wood, hardwood square dowels unfinished wooden strips from Yulejo. Organosolv-fractionated hardwood lignin from mixed biomass (*41*) was obtained from Lignol Innovations, Canada. TOCNs and CNCs were both obtained from the University of Maine Process Development Center.

Ink formulation

The organosolv-fractionated hardwood lignin has been thermally reprocessed at 180°C for devolatilization of gaseous products, and residual solvent. Specifically, powder lignin was sheared in a 350-cm^3

Downloaded from https://www.science.org on April 03, 2024

batch mixer of a Brabender polymer processing system at 180°C, 60 rpm rotor speed for 60 min to obtain devolatilized chunks that were then pulverized and used in this study. The lignin devolatilization step helps the consolidation of DIW printed layers during the heat treatment of the printed part. TOCN and 10.6 wt % aqueous solution of CNC were mixed with lignin at a ratio of 15:142:10 by weight of TOCN, CNC (aqueous), and lignin, respectively. Then, the mixture was placed in a Thinky Planetary Centrifugal Mixer (model AR 230), mixed in three cycles at 2000 rpm for 5 min, and then defoamed at 2200 rpm for 1 min. Last, the mixture is taken out and ready for printing.

Ink viscosity test

Rheological analysis was carried out on the ink formulation using the rotational ARES G2 Rheometer, courtesy of Rice University Shared Equipment Authority. This system modulates the shear rate and oscillation strain while recording the torque and normal force exerted on the ink between a cone and plate geometry. Flow and viscosity curves were obtained in strain-rate controlled measurement at shear rates from 0.05 to 100 s^{-1} at room temperature (25°C). Oscillatory amplitude sweeps were performed at an angular frequency of 1 Hz with the oscillation strain from 0.1 to 100%.

3D printing

The high-resolution 3D printer (Hyrel Engine HR) was used to print the wood ink formulation. The cold flow syringe head (SDS-60 Extruder) was used to extrude the ink at room temperature. The ink was loaded in a 60-ml Luer-lock syringe and shaken to ensure bubbles were removed. Smooth-flow tapered tips (Nordson EFD) of 25 gauge were used to resist clogging and printing discontinuity while dispensing the ink. The ink was printed on a silicone substrate to prevent the adhesion of the wood structure and build plate and facilitate detaching the printed object from the build plate. The Slic3r software was used to generate the G-code script based on the geometry and other parameters like extrusion width, printing speed, and layer height to determine the print path. The ink flow rate was tuned to facilitate smooth printing.

Freeze-drying

The printed samples were placed under dry ice for 30 min and then freeze-dried at −85°C, under less than 0.1-mbar pressure, for 48 hours using the FreeZone 4.5 Liter Benchtop Freeze Dry System. Instead of liquid nitrogen, dry ice was used to freeze the sample immediately after printing, before freeze-drying, to avoid cracking. Note that the temperature of liquid nitrogen is about −196°C (*52*), while that of dry ice is around −79°C (*53*), both of which are sufficient to freeze the water in the structure. We speculate that in the case of liquid nitrogen, the very steep thermal gradient results in a thermal shock, due to which the structures crack. With dry ice, the structures never cracked and yet were completely frozen.

Heat treatment

The unpressed samples were heated at 180°C immediately after freeze-drying. For samples that require hot pressing, the sample was preheated inside a metal mold at 180°C for 20 min, and then it was pressed with the system temperature maintained for another 10 min. For samples that needed double press, this process was repeated in both directions.

Mechanical testing

The compression and flexural tests were carried out on Instron 4505 and Instron 5982, respectively. The samples used for the compression test were 5 mm × 5 mm × 15 mm, and the loading rate was 0.3%/min, following the ASTM D143-94 standard test method. The flexural test samples had a square cross section of approximately 5 mm and a span length of 20 mm. The loading rate was 1 mm/min for these tests. In all compression tests, the loading direction was parallel to the orientation of the fibers of natural wood and the alignment direction of the layers of 3D-printed wood. The flexural test was carried out perpendicular to this direction. Each test was carried out on at least three samples, and the average data were plotted.

Thermogravimetric analysis

Thermal degradation of the samples and the individual components was measured by the Mettler Toledo TGA/DSC 3+ system from room temperature to 800°C at 1°C/s. The test was performed with nitrogen flow at 100 ml/min.

X-ray scattering

Characterization of the structural morphology at various stages in the printing process and printing direction was performed with x-ray scattering. Printed samples were characterized in solid form following the freeze-drying step. Samples were sectioned along prescribed directions to a thickness of ~2 mm to provide adequate scattering information by calculating the scattering length density of the highly oxygenated carbon atoms. To enable accurate attribution of scattering features to the correct phases in the printing ink, isolated lignin powder, TOCN, and hydrated CNCs were placed between two Kapton windows. For these samples, the intensity resulting from an empty Kapton cell was removed during background subtraction. Scattering experiments were performed with a Xeuss 3.0 (Xenocs, France) equipped with a D2+ MetalJet x-ray source (Ga Ka, 9.2 keV, $\lambda = 1.34$ Å). Two-dimensional images of the scattering patterns were collected on a PILATUS hybrid photon counting detector with a pixel dimension of 75 × 75 μm^2 (Dectris, Switzerland). The 2D SAXS images were circularly averaged and reduced in the form of intensity versus scattering vector (q), where $q = (4\pi \sin\theta)/\lambda$. All images were collected with background corrections and reduced using the XSACT software package (Xenocs, France).

Softening point characterization

To assess the softening point of the lignin material, a pellet was prepared by first adding ~2 g of raw lignin powder to a metal fixture. The fixture was then placed into a convection oven at 170°C for 30 min, removed, and consolidated under an applied pressure of 14 MPa. Lower thermal treatment temperatures of 130°C did not yield a conformal puck. The pellet was removed and placed within a parallel plate rheometer (TA Instruments, Discovery HR-3) using an 8-mm flat geometry. A 0.2 N compressive force was applied to the lignin puck along with a temperature ramp rate of 5°C/min.

Supplementary Materials

This PDF file includes:

Figs. S1 to S8

Tables S1 and S2

Other Supplementary Material for this manuscript includes the following:

Movie S1

Downloaded from https://www.science.org on April 03, 2024

REFERENCES AND NOTES

1. G. Wimmers, Wood: A construction material for tall buildings. *Nat. Rev. Mater.* **2**, 17051 (2017).
2. D. N. S. Hon, N. Shiraishi, *Wood and Cellulosic Chemistry, Revised, and Expanded* (CRC Press, ed. 0, 2000).
3. A. Cavalli, D. Cibecchini, M. Togni, H. S. Sousa, A review on the mechanical properties of aged wood and salvaged timber. *Construct. Build Mater.* **114**, 681–687 (2016).
4. K. Kránitz, W. Sonderegger, C.-T. Bues, P. Niemz, Effects of aging on wood: A literature review. *Wood Sci. Technol.* **50**, 7–22 (2016).
5. W. Sonderegger, K. Kránitz, C.-T. Bues, P. Niemz, Aging effects on physical and mechanical properties of spruce, fir and oak wood. *J. Cult. Herit.* **16**, 883–889 (2015).
6. E. Novaes, M. Kirst, V. Chiang, H. Winter-Sederoff, R. Sederoff, Lignin and biomass: A negative correlation for wood formation and lignin content in trees. *Plant Physiol.* **154**, 555–561 (2010).
7. R. H. Falk, D. B. McKeever, Recovering wood for reuse and recycling: A United States perspective, in *European COST E31 Conference: Management of Recovered Wood Recycling Bioenergy and other Options: Proceedings*, 22–24 April 2004, Thessaloniki (Univ. Studio Press, 2004), pp. 29–40.
8. M. Irle, F. Privat, L. Couret, C. Belloncle, G. Déroubaix, E. Bonnin, B. Cathala, Advanced recycling of post-consumer solid wood and MDF. *Wood Mater. Sci. Eng.* **14**, 19–23 (2019).
9. K. M. F. Hasan, P. G. Horváth, T. Alpár, Nanotechnology for waste wood recycling, in *Nanotechnology in Paper and Wood Engineering* (Elsevier, 2022), pp. 61–80.
10. A. Besserer, S. Troilo, P. Girods, Y. Rogaume, N. Brosse, Cascading recycling of wood waste: A review. *Polymers* **13**, 1752 (2021).
11. S. Beluns, S. Gaidukovs, O. Platnieks, G. Gaidukova, I. Mierina, L. Grase, O. Starkova, P. Brazdausks, V. K. Thakur, From wood and hemp biomass wastes to sustainable nanocellulose foams. *Ind. Crops Prod.* **170**, 113780 (2021).
12. M. Rajinipriya, M. Nagalakshmaiah, M. Robert, S. Elkoun, Importance of agricultural and industrial waste in the field of nanocellulose and recent industrial developments of wood based nanocellulose: A review. *ACS Sustainable Chem. Eng.* **6**, 2807–2828 (2018).
13. L. Couret, M. Irle, C. Belloncle, B. Cathala, Extraction and characterization of cellulose nanocrystals from post-consumer wood fiberboard waste. *Cellul.* **24**, 2125–2137 (2017).
14. O. Suchsland, G. E. Woodson, *Fiberboard Manufacturing Practices in the United States* (U.S. Department of Agriculture, Forest Service, 1987).
15. M. M. Rahman, A. N. Netravali, Advanced green composites using liquid crystalline cellulose fibers and waxy maize starch based resin. *Compos. Sci. Technol.* **162**, 110–116 (2018).
16. M. M. Rahman, A. N. Netravali, Micro-fibrillated cellulose reinforced eco-friendly polymeric resin from non-edible 'Jatropha curcas' seed waste after biodiesel production. *RSC Adv.* **6**, 47101–47111 (2016).
17. K. Wan, B. Tian, Y. Zhai, Y. Liu, H. Wang, S. Liu, S. Li, W. Ye, Z. An, C. Li, J. Li, T. D. James, Z. Chen, Structural materials with afterglow room temperature phosphorescence activated by lignin oxidation. *Nat. Commun.* **13**, 5508 (2022).
18. Q.-F. Guan, H.-B. Yang, Z.-M. Han, L.-C. Zhou, Y.-B. Zhu, Z.-C. Ling, H.-B. Jiang, P.-F. Wang, T. Ma, H.-A. Wu, S.-H. Yu, Lightweight, tough, and sustainable cellulose nanofiber-derived bulk structural materials with low thermal expansion coefficient. *Sci. Adv.* **6**, eaaz1114 (2020).
19. F. Yuan, Y. Huang, J. Qian, M. M. Rahman, P. M. Ajayan, D. Sun, Free-standing SnS/carbonized cellulose film as durable anode for lithium-ion batteries. *Carbohydr. Polym.* **255**, 117400 (2021).
20. J. Ralph, C. Lapierre, W. Boerjan, Lignin structure and its engineering. *Curr. Opin. Biotechnol.* **56**, 240–249 (2019).
21. D.-W. Cho, K. Yoon, Y. Ahn, Y. Sun, D. C. W. Tsang, D. Hou, Y. S. Ok, H. Song, Fabrication and environmental applications of multifunctional mixed metal-biochar composites (MMBC) from red mud and lignin wastes. *J. Hazard. Mater.* **374**, 412–419 (2019).
22. R.-C. Sun, Lignin source and structural characterization. *ChemSusChem* **13**, 4385–4393 (2020).
23. Y. Tang, H. Yang, S. Vignolini, Recent progress in production methods for cellulose nanocrystals: Leading to more sustainable processes. *Adv. Sustain. Syst.* **6**, 2100100 (2022).
24. M. A. S. R. Saadi, A. Maguire, N. T. Pottackal, M. S. H. Thakur, M. M. Ikram, A. J. Hart, P. M. Ajayan, M. M. Rahman, Direct ink writing: A 3D printing technology for diverse materials. *Adv. Mater.* **34**, e2108855 (2022).
25. S. M. Sajadi, C. F. Woellner, P. Ramesh, S. L. Eichmann, Q. Sun, P. J. Boul, C. J. Thaemlitz, M. M. Rahman, R. H. Baughman, D. S. Galvão, C. S. Tiwary, P. M. Ajayan, 3D printed tubulanes as lightweight hypervelocity impact resistant structures. *Small* **15**, e1904747 (2019).
26. S. M. Sajadi, L. Vásárhelyi, R. Mousavi, A. H. Rahmati, Z. Kónya, Á. Kukovecz, T. Arif, T. Filleter, R. Vajtai, P. Boul, Z. Pang, T. Li, C. S. Tiwary, M. M. Rahman, P. M. Ajayan, Damage-tolerant 3D-printed ceramics via conformal coating. *Sci. Adv.* **7**, eabc5028 (2021).
27. A. K. Das, D. A. Agar, M. Rudolfsson, S. H. Larsson, A review on wood powders in 3D printing: Processes, properties and potential applications. *J. Mater. Res. Technol.* **15**, 241–255 (2021).
28. Forust, *Forust*. www.forust.com/.
29. D. Correa, A. Papadopoulou, C. Guberan, N. Jhaveri, S. Reichert, A. Menges, S. Tibbits, 3D-printed wood: Programming hygroscopic material transformations. *3D Print. Addit. Manuf.* **2**, 106–116 (2015).
30. S. Zhang, M. Li, N. Hao, A. J. Ragauskas, Stereolithography 3D printing of lignin-reinforced composites with enhanced mechanical properties. *ACS Omega* **4**, 20197–20204 (2019).
31. A. Maguire, N. Pottackal, M. A. S. R. Saadi, M. M. Rahman, P. M. Ajayan, Additive manufacturing of polymer-based structures by extrusion technologies. *Oxf. Open Mater. Sci.* **1**, itaa004 (2020).
32. L.-S. Ebers, A. Arya, C. C. Bowland, W. G. Glasser, S. C. Chmely, A. K. Naskar, M.-P. Laborie, 3D printing of lignin: Challenges, opportunities and roads onward. *Biopolymers* **112**, e23431 (2021).
33. B. Jiang, H. Jiao, X. Guo, G. Chen, J. Guo, W. Wu, Y. Jin, G. Cao, Z. Liang, Lignin-based materials for additive manufacturing: Chemistry, processing, structures, properties, and applications. *Adv. Sci.* **10**, e2206055 (2023).
34. B. Jiang, Y. Yao, Z. Liang, J. Gao, G. Chen, Q. Xia, R. Mi, M. Jiao, X. Wang, L. Hu, Lignin-based direct ink printed structural scaffolds. *Small* **16**, e1907212 (2020).
35. J. Yang, X. An, L. Liu, S. Tang, H. Cao, Q. Xu, H. Liu, Cellulose, hemicellulose, lignin, and their derivatives as multi-components of bio-based feedstocks for 3D printing. *Carbohydr. Polym.* **250**, 116881 (2020).
36. X. Zhang, M. Morits, C. Jonkergouw, A. Ora, J. J. Valle-Delgado, M. Farooq, R. Ajdary, S. Huan, M. Linder, O. Rojas, M. H. Sipponen, M. Österberg, Three-dimensional printed cell culture model based on spherical colloidal lignin particles and cellulose nanofibril-alginate hydrogel. *Biomacromolecules* **21**, 1875–1885 (2020).
37. F. R. Gleuwitz, G. Sivasankarapillai, G. Siqueira, C. Friedrich, M.-P. G. Laborie, Lignin in bio-based liquid crystalline network material with potential for direct ink writing. *ACS Appl. Bio Mater.* **3**, 6049–6058 (2020).
38. F. R. Gleuwitz, C. Friedrich, M.-P. G. Laborie, Lignin-assisted stabilization of an oriented liquid crystalline cellulosic mesophase, part A: Observation of microstructural and mechanical behavior. *Biomacromolecules* **21**, 1069–1077 (2020).
39. T. Liebrand, "3D printed fiber reinforced lignin: Exploring the options to use wood in an additive manufacturing process," thesis, Delft University of Technology, Delft, Netherlands (2018).
40. C. Bierach, A. A. Coelho, M. Turrin, S. Asut, U. Knaack, Wood-based 3D printing: Potential and limitation to 3D print building elements with cellulose & lignin. *Archit. Struct. Constr.* **3**, 157–170 (2023).
41. N. A. Nguyen, K. M. Meek, C. C. Bowland, A. K. Naskar, Responsive lignin for shape memory applications. *Polymer* **160**, 210–222 (2019).
42. J. Song, C. Chen, S. Zhu, M. Zhu, J. Dai, U. Ray, Y. Li, Y. Kuang, Y. Li, N. Quispe, Y. Yao, A. Gong, U. H. Leiste, H. A. Bruck, J. Y. Zhu, A. Vellore, H. Li, M. L. Minus, Z. Jia, A. Martini, T. Li, L. Hu, Processing bulk natural wood into a high-performance structural material. *Nature* **554**, 224–228 (2018).
43. A. Paajanen, A. Zitting, L. Rautkari, J. A. Ketoja, P. A. Penttilä, Nanoscale mechanism of moisture-induced swelling in wood microfibril bundles. *Nano Lett.* **22**, 5143–5150 (2022).
44. N. Cohen, G. Ochbaum, Y. Levi-Kalisman, R. Bitton, R. Yerushalmi-Rozen, Polymer-induced modification of cellulose nanocrystal assemblies in aqueous suspensions. *ACS Appl. Polym. Mater.* **2**, 732–740 (2020).
45. T. Yoshida, D. Muto, T. Tamai, S. Suzuki, Improvement of strength and energy absorption properties of porous aluminum alloy with aligned unidirectional pores using equal-channel angular extrusion. *Metall Mater Trans* **49**, 2463–2470 (2018).
46. Y. Su, J. Zhu, X. Long, L. Zhao, C. Chen, C. Liu, Statistical effects of pore features on mechanical properties and fracture behaviors of heterogeneous random porous materials by phase-field modeling. *Int. J. Solids Struct.* **264**, 112098 (2023).
47. M. Borrega, L. J. Gibson, Mechanics of balsa (*Ochroma pyramidale*) wood. *Mech. Mater.* **84**, 75–90 (2015).
48. M. M. Rahman, A. N. Netravali, Aligned bacterial cellulose arrays as "green" nanofibers for composite materials. *ACS Macro Lett.* **5**, 1070–1074 (2016).
49. Y. Zhao, J. Li, Excellent chemical and material cellulose from tunicates: Diversity in cellulose production yield and chemical and morphological structures from different tunicate species. *Cellul.* **21**, 3427–3441 (2014).
50. A. Kumar, Y. S. Negi, V. Choudhary, N. K. Bhardwaj, Characterization of cellulose nanocrystals produced by acid-hydrolysis from sugarcane bagasse as agro-waste. *J. Mater. Phys. Chem.* **2**, 1–8 (2014).
51. D. Watkins, M. Nuruddin, M. Hosur, A. Tcherbi-Narteh, S. Jeelani, Extraction and characterization of lignin from different biomass resources. *J. Mater. Res. Technol.* **4**, 26–32 (2015).
52. T. A. Scott, Solid and liquid nitrogen. *Phys. Rep.* **27**, 89–157 (1976).
53. Dry ice, *Wikipedia* (2023); https://en.wikipedia.org/w/index.php?title=Dry_ice&oldid=1187650587.

Downloaded from https://www.science.org on April 03, 2024

Acknowledgments: We thank A. Z. Khater for suggestions and J. Li for help with the art in Figure 1. We also thank R. Purvis, Moody Center for the Arts, Rice University, for help with making the molds for hot-pressing samples. We acknowledge the support of the Rice University Shared Equipment Authority for using the Helios SEM, ARES G2 Rheometer, and the FreeZone 4.5 Liter Benchtop Freeze Dry System; and the Rice University Materials Science and NanoEngineering department for continual support. **Funding:** A.K.N. and L.T.K. acknowledge support from the U.S. Department of Energy, Office of Science, Basic Energy Sciences, Materials Sciences, and Engineering Division under FWP ERKCK60. **Author contributions:** M.M.R. and M.S.H.T. conceived the concept and designed the experiments. M.S.H.T. and C.S. did the fabrication, postprocessing, compression tests, and characterizations. P.M.A. assisted in providing facilities and scientific discussion. L.T.K. and A.K.N. provided the lignin and conducted WAXS and softening point characterization. L.T.K. also carried out the flexure tests. M.A.S.R.S. conducted the fracture surface analysis. M.S.H.T., M.A.S.R.S., and C.S. wrote the manuscript. M.D.M. performed the TEM characterizations. M.M.R. supervised the project. All authors contributed to the scientific discussion and editing of the manuscript. **Competing interests:** The authors declare that they have no competing interests. **Data and materials availability:** All data needed to evaluate the conclusions in the paper are present in the paper and/or the Supplementary Materials.

Submitted 15 August 2023
Accepted 9 February 2024
Published 15 March 2024
10.1126/sciadv.adk3250

Downloaded from https://www.science.org on April 03, 2024